Cyclic Performance of TR-CFT Columns under Flexural Loadings

J. W. Park.[1], J. H. Kim.[2] and J. H. Hur.[3]

[1] *PhD, Dept. of Architecture, Hong Ik University, Seoul, Korea.*
[2] *PhD, Korea Railroad Research Institute, Uiwang, Korea.*
[3] *Doctoral degree student, University of Science & Technology, Daejeon, Korea.*
Email: anm21c@ hanmail.net.

ABSTRACT :

This paper presents an experimental test and analytical modeling for CFT concrete filled steel tubes (CFT) and TR-CFT (Transversely- Reinforced Concrete-Filled Steel Tubes) under combined axial compression and cyclic loading. Modified P-M curves with the confining effect are also presented to predict the flexural capacity of CFT and TR-CFT. Test results were found to be in good agreement with the predicted values from the modified P-M curves.

KEYWORDS: CFT, TR-CFT, Composite column, Confinement, P-M curve

1. Introduction

Recently, Concrete-Filled Steel Tubes (CFTs) have been used in many structural applications, such as high-rise building's columns and bridge piers. As a composite structural system, the conventional CFT columns provide composite effects due to the advantages of having two materials; disadvantages can be compensated for. Because the steel tubes can be used as a formwork, economic effects can be also expected in construction fields. However, the conventional CFT columns have their own disadvantages. As demonstrated in cyclic load tests for CFT columns, local buckling may occur at the end of columns followed by a reduction of strength of steel tubes and the crushing of internal concrete.

To solve this problem, this research first not only presents a new structural system called TR-CFT (Transversely- Reinforced Concrete-Filled Steel Tubes) but also gives results of beam-column tests for TR-CFT columns. In the TR-CFT columns, Carbon Fiber Sheets (CFS) were used as additional confinement materials to delay or control local buckling at the end of CFT columns; columns were wrapped at the potential plastic local buckling zone. The various parameters are compressive strength of concrete and the number of CFS layers. Eight specimens were made in the experimental parameter planning. From beam-column tests, the hysteretic curve, flexural moment capacity, yield stiffness, stiffness degradation, and ductility capacity are compared and analyzed between the rectangular CFT and TR-CFT columns.

Second, according to the current CFT codes, such as ACI code, because the code does not consider the contribution of the concrete confining effect, the flexural capacity value evaluated by the ACI code is over-conservative. Therefore, in this study, stress-strain curves for confining concrete are evaluated by using the Mander and Monti's theories. From these curves, modified flexural capacity equations for CFT and TR-CFT considering concrete confining effect are proposed in this research. Modified P-M curves for CFT and TR-CFT columns are also compared with experimental results.

2. Experimental Results and Discussions

Eight CFT and TR-CFT specimens were made and beam-column tests were conducted. The specimen had a rectangular section with a width of 125 mm, and a height of 550 mm. The thickness of steel tube was 4.5 mm. The CFS had a width of column (125mm) which was wrapped at the end of column.

The yield strength of the steel tube was 427 MPa in the tension test. The results of compressive strength for concrete were 24.3 MPa (R2), 39.9 MPa (R4) and 53.0 MPa (R5). The rupture strength of CFS was 3500 MPa and the ultimate strain of CFS was 1.5 %. The nominal thickness was 0.111mm/ layer.

The cyclic loading was controlled by ANSI/ AISC 341-02 beam-column's cyclic loading programming

(ANSI/ AISC 2002). The constant axial load value was 0.3 times the ultimate compression strength evaluated by AISC-LRFD provision (AISC 2001).

The various parameters in this research were concrete compressive strength and the number of CFS layer.

2.1. Specimen failure procedure

Figure 1 shows the final failure shapes for R5N specimen. The failure procedure of all specimens is as follows. For the conventional CFT specimens such as R2N, R4N, and R5N, the local buckling was first observed at the end of columns during the loading cycles corresponding to a peak drift ratio of 3.0%, and then the local buckling zone gradually expanded; columns finally failed during loading cycle at 4.0% drift.

Figure 1 Failure procedure for conventional CFT column (R5N)

On the other hand, the specimens wrapped with over 2 layers of CFS such as R5F-2 and R5F-3, the rupture of CFS first observed at the 4.0% drift level and the specimens failed at 6.0 % drift level, as shown in Figure 3. The specimens were able to endure the loading cycles corresponding to drift ratio of 6.0 % due to the delay of local buckling by additional confinement of CFS.

Figure 2 Failure procedure for TR-CFT column (R5F-3)

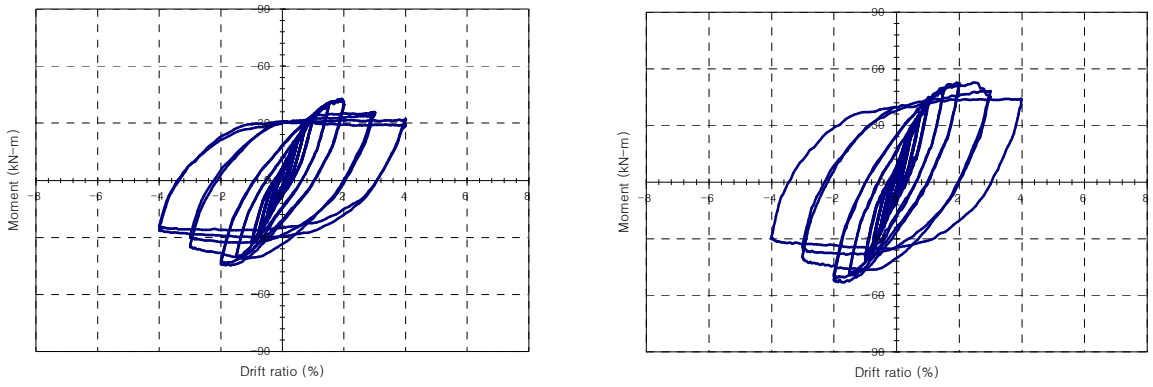

(a) R2N (f'_c =24MPa, CFS layer : 0 ply)

(b) R2F-1 (f'_c =24MPa, CFS layer : 1 ply)

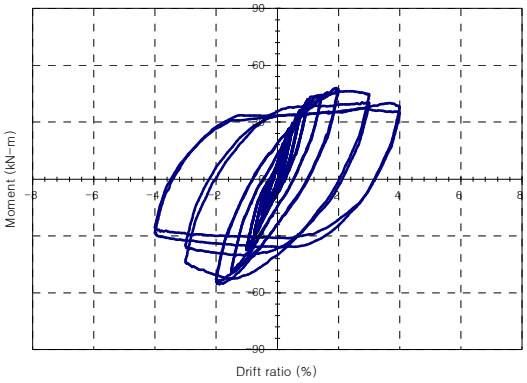

(c) R4N (f'_c =40MPa, CFS layer : 0 ply)

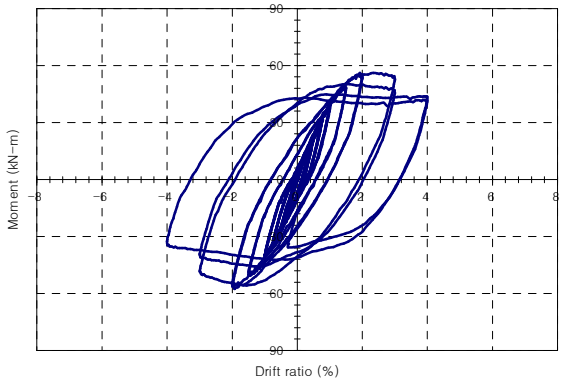

(d) R4F-1 (f'_c =40MPa, CFS layer : 1 ply)

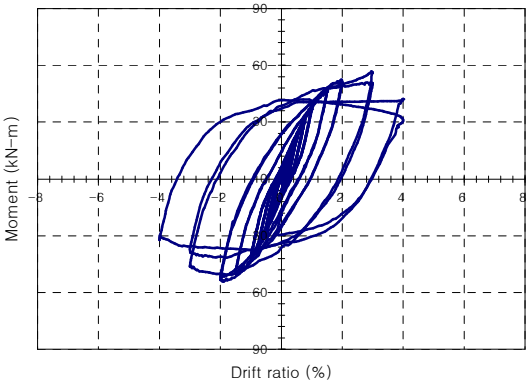

(e) R5N (f'_c =50MPa, CFS layer : 0 ply)

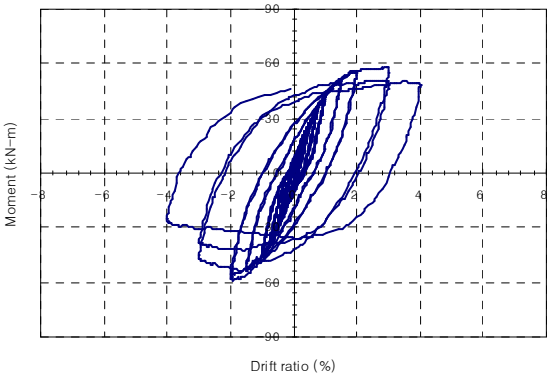

(f) R5F-1 (f'_c =50MPa, CFS layer : 1 ply)

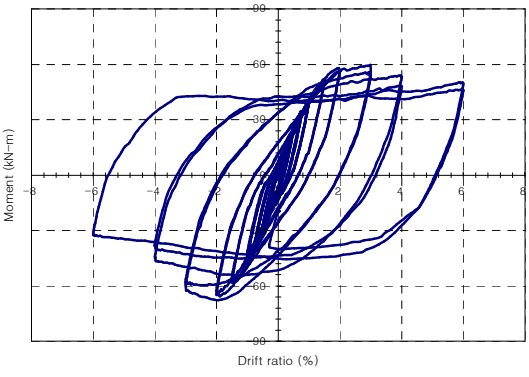

(g) R5F-2 (f'_c =50MPa, CFS layer : 2 ply)

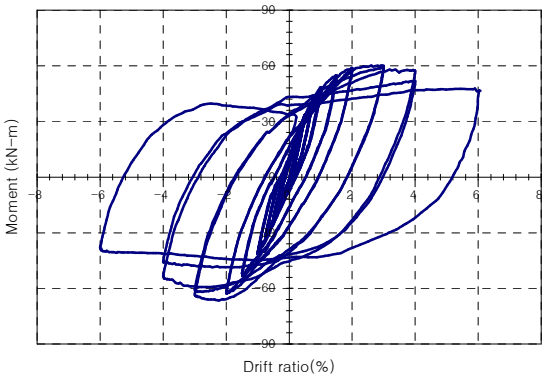

(h) R5F-3 (f'_c =50MPa, CFS layer : 3 ply)

Figure 3 Moment-drift ratio hysteretic curves for specimens.

As shown in Figure 3 (a), (c) and (e), the conventional CFT columns (R2N, R4N, and R5N) behaved well until the drift ratio of 3.0 % stage (For R2N: 2.0%). At that stage, the peak moment of specimen was observed. However, the local buckling occurred after the peak moment stage caused the reduction of moment capacity of specimen.

In Figure 3 (h), the hysteretic curve of R5F-3 specimen is shown. The peak moment of specimen was also observed at the stage of 3.0 % However, a dramatic reduction of moment capacity was observed at the drift ratio of 6.0 %. From Figure (g) and (h), TR-CFT columns wrapped with over two layers of CFS developed ultimate drift ratios equal to 6.0 %. For R5F-2, 3 specimens, it was shown that a larger deformability for TR-CFT columns could be observed for TR-CFT columns than for the conventional CFT columns. Comparing the results of CFT and TR-CFT columns, significantly improved seismic behaviors could be seen in TR-CFT columns due to the delayed local buckling provided by additional confinement of CFS.

Figure 4 shows the skeleton curves of all specimens.

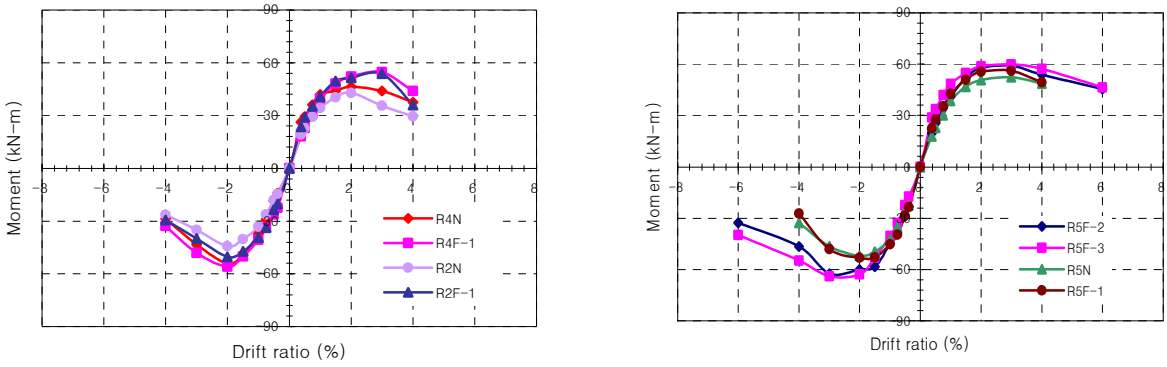

Figure 4 Skeleton curves of specimens

2.2. Yield stiffness and stiffness degradation

The concept used to evaluate yield stiffness is presented in Figure 5. From the skeleton curve, the yield point can be defined the intersection of line (a) and (c). The yield stiffness is defined as Equation (3-1).

$$K_y = \frac{M_y}{\theta_y} \tag{2-1}$$

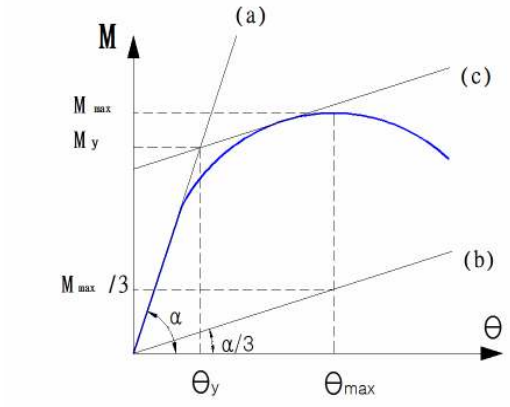

Figure 5 Definition of yield point

In table 2.1, the stiffness values of all specimens are presented.

From the result, it is evident that the stiffness of CFT was similar to that of TR-CFT wrapped by 1 layer of CFS. However, for the specimens with 50MPa concrete, the stiffness increased up to 25% with the increased CFS reinforcement ratio.

Table 2.1 Yield stiffness of specimens

Specimen	(+)direction	(-)direction	Average (kN-m)
R2N	49.4	38.7	44.1
R2F-1	44.9	49.0	47.0
R4N	49.1	48.5	48.8
R4F-1	47.9	56.1	52.0
R5N	43.3	58.2	50.8
R5F-1	47.7	55.2	51.5
R5F-2	54.4	64.3	59.4
R5F-3	74.9	52.1	63.5

Figure 7 shows the stiffness degradation of the specimens under cyclic loading. The stiffness (K_i) at the peak of the ith loading cycle is defined as Equation (2-2).

$$K_i = \frac{M_i}{\theta_i} \tag{2-2}$$

Where, M_i and θ_i are the peak moment and drift ratio of the ith cycle.

As shown in Figure 6, peak stiffness (K_i) degrades with the increase of drift ratio, and tends to stabilize corresponding to the large drift ratio. From the skeleton curve of stiffness degradation, it is evident that the stiffness of all specimens is similar even though there are slight differences between CFT columns and TR-CFT columns.

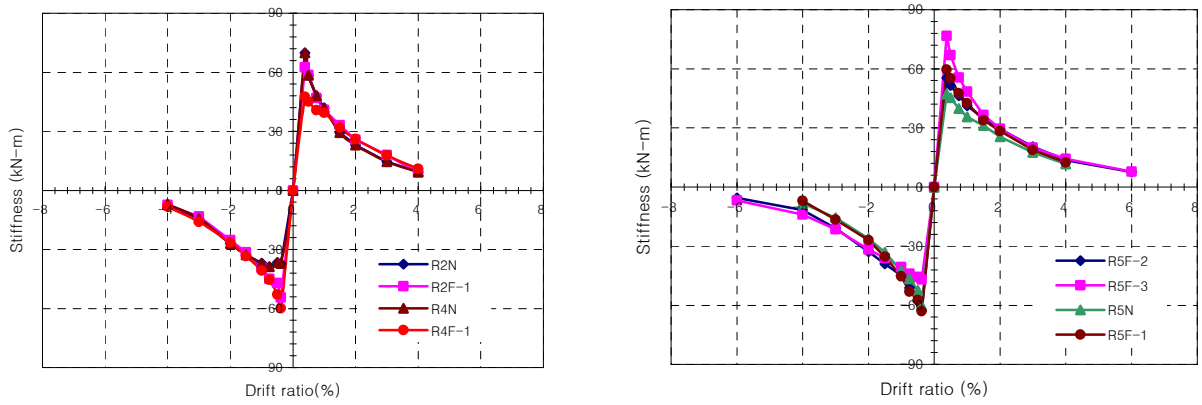

Figure 6 The skeleton curves of stiffness degradation of specimens

2.3. Ductility

Ductility capacity is an important consideration in seismic design of structural members. In this research, the definition of ductility obtained from the skeleton curve is the ratio of drift corresponding to 0.9 times drift occurring at maximum moment to drift at first yielding point. This ductility can be defined as Equation (2-3).

$$\mu = \frac{\theta_{90}}{\theta_y} \tag{2-3}$$

Figure 7 shows the ductility capacity of all specimens ratio to R2N specimen.

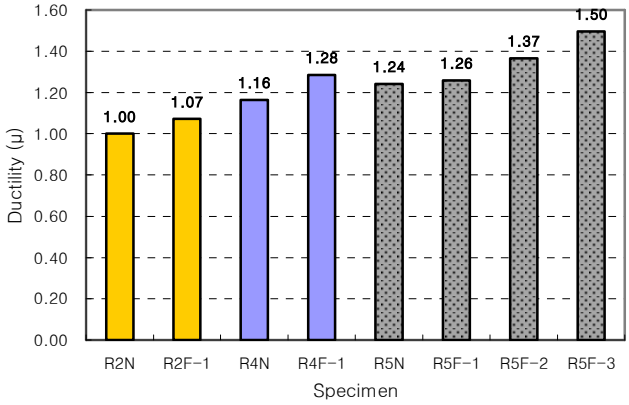

Figure 7 Ductility capacity of specimens as a ratio of R2N specimen

As shown in Figure 7, the ductility capacity improves with increasing concrete compressive strength and CFS reinforcement ratio. There is little ductility difference between RN group specimens and RF-1 group specimens. However, for the R5 group specimens (R5N, R5F-1, R5F-2, and R5F-3), the ductility capacity is dramatically improved with the increased CFS reinforcement ratio. This is because the additional CFS confinement can delay the local buckling occurring at the end of the conventional CFT columns. From section 2.2 and 2.3, it is evident that TR-CFT columns focus on ductility enhancement rather than stiffness improvement. In general, because seismic design demands good ductility capacity, TR-CFT columns can be expected to be good alternative members for CFT columns.

3. P-M interaction curve for CFT and TR-CFT columns

3.1. CFT column design in ACI code

P-M curve provides the behavior of columns under compression and flexural loading. In this study, the ACI code for CFT columns will be considered. Figure 8 (a) shows the design concept of the ACI code for CFT columns (ACI 2005). A continuous steel tube in a section is transformed and distributed to discrete equivalent steel bar. The extreme ultimate strain value at compression section is 0.003 and a concrete stress block is used as $0.85f'_c$. Because the concrete filled in the steel tube is laterally confined, the strength and ductility of the concrete must be greater than that of the unconfined concrete. However, since the ACI code does not consider the contribution of the concrete confining effect, the flexural capacity value evaluated by the ACI code is actually over-conservative. Therefore, the ACI code is problematic for design guidance.

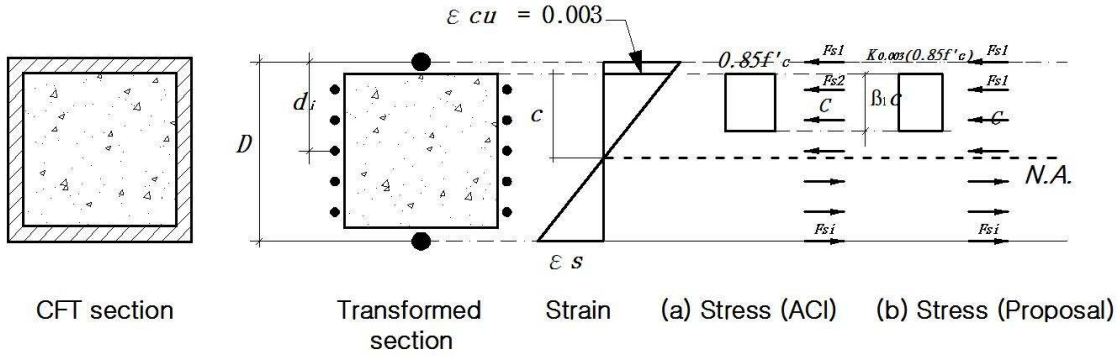

Figure 8 ACI and Proposed design concept for CFT and TR-CFT columns

3.2. Confined concrete stress-strain model

In this research, confined concrete a stress-strain model is used to consider for the contribution of concrete confining effect filled in steel tubes. For the CFT columns, Mander's confined concrete stress-strain model is used (Mander 1988). For TR-CFT model, Monti's confined concrete stress-strain model is used as confined concrete stress-strain model (Monti 1999). Each stress-strain model is shown in Figure 9.

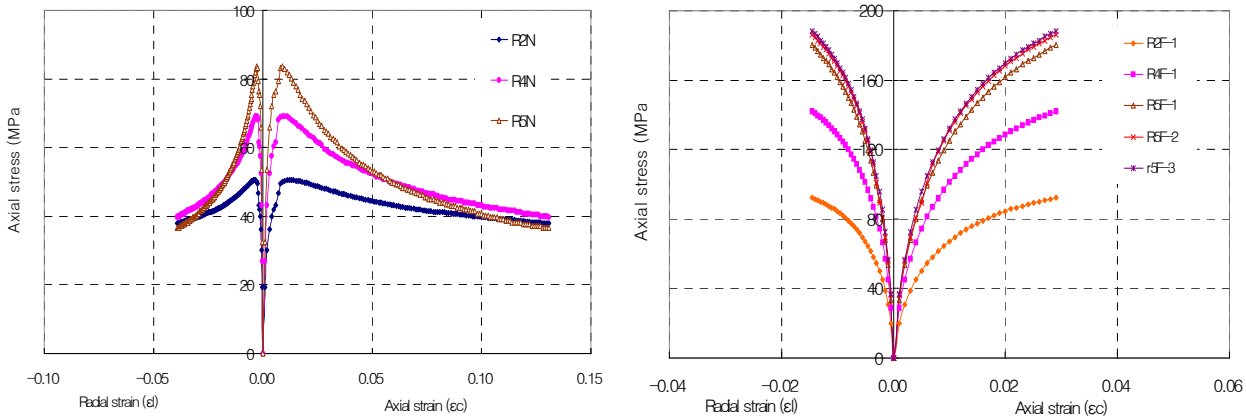

(a) CFT columns (b) TR-CFT columns

Figure 9 Confined concrete stress-strain model of specimens

3.3. Modified P-M curve of specimens

In Figure 10, the modified P-M curves of CFT and TR-CFT columns considering the confining effect are presented. To consider the concrete strength improvement effect by the confining effect, this study presents a confinement coefficient $K_{0.003}$(refer to Figure 8 (b)). The coefficient is defined as the ratio of confined concrete strength to unconfined concrete strength at compressive strain value 0.003.

The assumption for the design is as follows:

① The ultimate strain of concrete is 0.003.
② Plane sections before bending remain plane after bending.
③ The concrete has no tensile strength.
④ Concrete, steel tube, and CFS behave as a composite member.
⑤ Other design assumption is similar to the ACI design concept.

By applying the confining effect, an internal moment corresponds to a compression at the top face is expressed as Equation (3-1).

$$M_n = K_{0.003}(0.85f'_c)(a)(D-2t)(\frac{D}{2}-\frac{a}{2})+\sum_{i=1}^{n}A_{si}f_{si}(\frac{D}{2}-d_i) \quad (3\text{-}1)$$

Where, $a=\beta_1 c$, $-f_y \le f_{si} \le f_y$, t : thickness of steel tube

The axial load capacity, P_n for the assumed strain distribution is the summation of the axial force and the total axial force is expressed as Equation (3.2).

$$P_n = K_{0.003}(0.85f'_c)(aD)+\sum_{i=1}^{n}A_{si}f_{si} \quad (3\text{-}2)$$

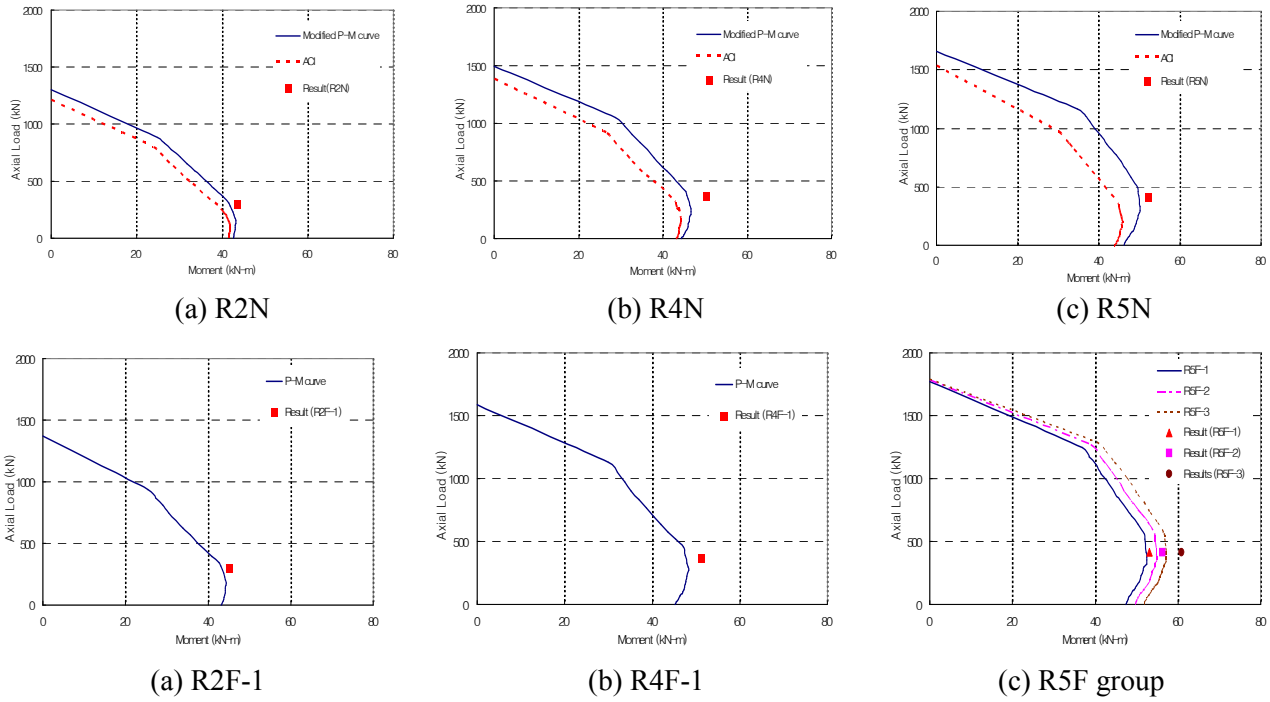

(a) R2N (b) R4N (c) R5N

(a) R2F-1 (b) R4F-1 (c) R5F group

Figure 10 Modified P-M curves of specimens

As shown Figure 10 (a), (b), and (c), by applying the confining effect, the modified P-M curve of CFT columns show improved results compared to the P-M curves evaluated by the current ACI code. It can also be seen from Figure 10 (c), (d), and (e) that test results for TR-CFT columns are found to be in good agreement with the predicted values when considering confining effect. This modified P-M curve can be expected to predict exact design values for CFT and TR-CFT columns under axial and flexural loadings.

4. Conclusion

1) CFT and TR-CFT columns' beam-column tests were conducted. By wrapping CFS at potential local buckling zone, local buckling could be delayed and flexural capacity and ductility capacity of TR-CFT columns improved more than did those of conventional CFT columns.

2) Modified P-M curves considering the confining effect are proposed in this research. The modified P-M curve of CFT columns shows improved results compared to the P-M curves evaluated by the current ACI code.

3) The P-M curves of TR-CFT are also proposed. By analyzing with the experimental results, test results for TR-CFT columns are found to be in good agreement with the predicted values.

REFERENCES

AISC, (2001), Manual of Steel Construction-Load Resistance Factor Design, American Institute of Steel Construction.

ANSI/ AISC 341-02, (2002), Seismic Provisions for Structural Steel Buildings, pp 40-41.

ACI Committee 318, (2005), Building Requirements for Structural Concrete and Commentary, American Concrete Institute.

J. W. Park., J. H. Kim., Y. K. Hong., G.S. Hong., (2007), An Experimental Study on TR-CFT Columns subjected to Axial Force and Cyclic Lateral Loads., *Journal of Korean Society of Steel Construction,* **Vol. 19, No 4**, pp 403-412.

J. B. Mander., M. J. N. Priestley., R. Park., (1988), Theoretical Stress-Strain Model for Confined Concrete., *Journal of Structural Engineering, ASCE,* **Vol. 114, No. 8**, pp 1804-1826.

M.R. Spoelstra., G. Monti., (1999), FRP-Confined Concrete Model., *Journal of Composite and Construction, ASCE,* **Vol. 3, No. 3**, pp 143-150.

J. G. Macgregor., (2005), Reinforced Concrete Mechanics and Design, Prentice Hall, U.S.A., pp 429-441.